

Towards Obtaining All Possible Contacts — Growing A Polyhedron by its Location Uncertainty*

Jing Xiao and Lixin Zhang
Computer Science Department
University of North Carolina - Charlotte
Charlotte, NC 28223
xiao@uncc.edu, lizhang@uncc.edu

Abstract

A large number of robotic tasks require precision and thus the dealing with uncertainties. The effects of various uncertainties often manifest to location (i.e., position and orientation) uncertainties of objects. Thus, an important problem that often arises is how to assess the region that an object may occupy in the presence of uncertainties. This paper addresses the problem by describing how to grow exactly an arbitrary polyhedral object in the three-dimensional Cartesian space by its position and/or orientation uncertainties. Three types of related regions for the object are described: (1) the *grown regions*, regions possibly occupied by the object due to uncertainties in its position, orientation, or both, (2) the *grown shell regions*, regions possibly occupied by the boundary (surfaces) of the object due to uncertainties in its position, orientation or both, and (3) the *core regions*, regions (which could be empty) definitely occupied by the object in spite of uncertainty. The exact representations introduced in this paper can serve as benchmarks against which efficient but approximate algorithms may be evaluated. A particularly important application of the grown shell regions is in obtaining the set of all possible topological contacts among polyhedral objects due to location uncertainties. Such a set can serve as a basis from which more precise contact information can be extracted by additional sensing means, such as vision and force/moment sensing. The approach for this application and its implementation is introduced and discussed.

1 Introduction

Certain uncertainties in a robotic operation environment are intrinsic and inevitable, for instance, the modeling and sensing uncertainties of a robot and the modeling and

*This research is supported by a National Science Foundation grant under number IRI-9210423.

sensing uncertainties of the objects to be handled by the robot or in the environment. Dealing with such uncertainties is crucial for robotic applications on tasks with high-precision or low-tolerance requirement, such as assembly operations, planning and navigation in crowded environments, precision material handling, etc. In many cases, the effect of these uncertainties manifests to location (i.e., position and orientation) uncertainties of objects, which may result in undesired collisions or contacts among objects (including robot) during a robotic operation. The *increased* risk of collision due to location uncertainties of objects can be likened to, as we observe, increased sizes of objects in the same environment. This suggests us to link the location uncertainties of an object to the enlargement of its size, that is, to find the region that the object may occupy if its location uncertainty is taken into account. We call this process *growing an object by its location uncertainty*. Finding the grown region of an object by its location uncertainty could be useful in *predicting* collisions and thus *preventing* unintended collisions due to uncertainties during motion planning (see Section 8), and most importantly, can play a major role, once a collision occurs, in automatically recognizing the topological contact in the presence of location uncertainties of the objects involved.

Our concept and approach of growing an object by its location uncertainty is novel in a number of ways. First, our approach decouples the effects of position and orientation uncertainties and grows an object through growing its every (boundary) surface element, i.e., every face, edge, and vertex, exactly. The decoupling of the effects of position and orientation uncertainties makes it possible for exact growth, i.e., the grown region computed is the least upper bound of the uncertain region that the object’s surface element may occupy due to location uncertainty. Or more intuitively, the region is not “rounded out”: all contours and concavities are preserved. This distinguishes our approach from resembling the defining of tolerance zones for an object’s feature to accommodate its uncertainty in geometric tolerancing[18]. We have a good reason: the exactness of a grown region is extremely useful in accurately estimating the possible collisions among objects and furthermore, the possible *types* of topological contacts among objects, in the presence of location uncertainties. It is, however, important to note that the exact grown regions may not be easy to compute due to the lack of efficient algorithms and thus approximate representations may be implemented (see Section 7.2). The significance of the exact analytical representation, then, is to serve as a benchmark against which different approximate representations can be evaluated.

It is also important to note that unlike in geometric tolerancing, we currently do not consider the uncertainty in the shapes of objects, although since we grow an object element by element, such uncertainty could also be accommodated rather easily.

Our approach of growing an object through its surface elements provides great convenience and flexibility. From the descriptions of grown regions of individual surface elements, the following three types of regions can be described easily: (1) the *grown regions* of the object, as the regions possibly occupied by the object due to

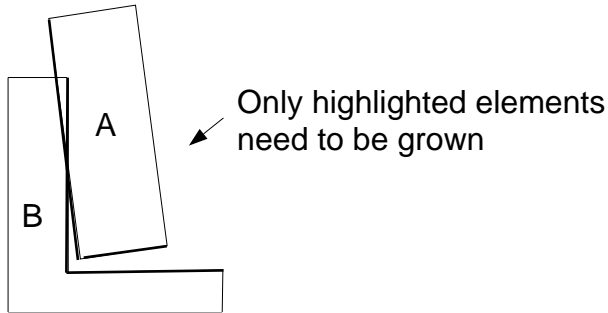


Figure 1: A 2-D example to show that partial growth is sufficient

uncertainty in its position, orientation, or both, (2) the *grown shell regions* of the object, as the regions possibly occupied by the boundary (surfaces) of the object due to uncertainties in its position, orientation, or both, and (3) the *core regions* of the object, as the regions (which could be empty) definitely occupied by the object in spite of uncertainties in its position, orientation, or both. In addition, this “modular” approach of growth naturally encourages (a) parallel growth of elements and (b) partial or local growth of an object to gain efficiency. Note that it is not always necessary to grow an object entirely; for instance, to obtain all possible contacts between two objects based on their estimated locations, only those faces of the two objects “facing” each other and the related edges and vertices need to be grown to take into account uncertainties (Fig. 1). Most importantly, growing an object element by element makes the method very general and applicable to convex and nonconvex polyhedra alike regardless the location of an object’s reference frame.

Finally, our method of growing an object takes place in the 3-D Cartesian space rather than in some other object’s configuration space[15, 16] to facilitate the recognition of topological contacts. As the result, the regions obtained are independent of the configuration and the shape of some other object.

Our work is particularly motivated by the need of automatic contact recognition in the presence of uncertainties. Automatic contact recognition is crucial for part-mating or assembly tasks where both task descriptions and operations are contact-based (see, for example, [1, 19, 13]), especially because of uncertainties. First, because of uncertainties, unintended contact between the part held (by the manipulator) and other parts in the environment can occur. Thus it is necessary to be able to recognize such a contact and to distinguish unintended contacts from intended ones, such as the contacts which define the goal state of an assembly. Secondly, the recognition task itself is also much complicated by the presence of uncertainties, even if the environment can be well controlled and structured in the sense that the models of all objects and fixtures are known, and their locations are either fixed or can be sensed. Such recognition task in the presence of uncertainties is especially difficult if the objects in contact are nonconvex.

Among the many attempts to determining contact states or constraints [4, 6, 2,

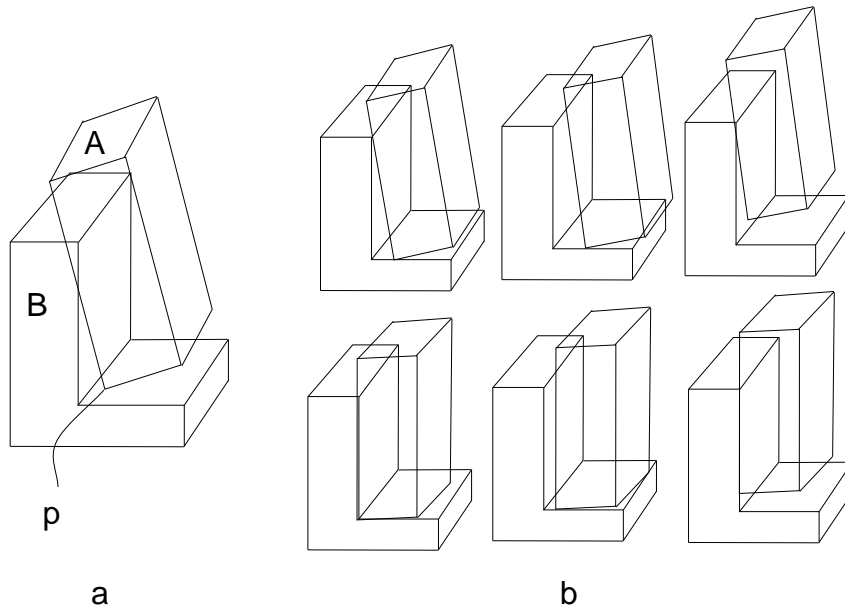


Figure 2: A , B and their possible relationships

20, 11, 24, 25, 12, 7, 17], only a few addressed the effect of uncertainties in contact recognition and were based almost universally on the approach of hypotheses-and-tests. Particularly, Desai and Volz[4, 5] used force/moment sensing data and Xiao and Su[25] used vision sensing to verify the contact hypotheses — a set of *possible* topological contact situations taking into account uncertainties. Spreng[20] used test motions for verifying contact hypotheses in terms of motion freedoms.

Clearly, a key problem is how to obtain effectively the initial contact hypotheses in the first place. In[24], Xiao specifically defined the problem as how to obtain the possible set of topological contact situations from the position/orientation sensing data of the objects in contact, taking into account sensing uncertainties. This problem is in itself a difficult one. The complex nature of the problem is best illustrated through an example. Suppose that two polyhedral solids A and B are in collision and that their geometrical models and sensed locations are known. An intersection relationship between A and B can be derived[3, 8, 21], which may not be pure contact relationship due to sensing uncertainties. The derivation may yield intrusions of one object into the other, absence of some contact points or no contact at all between the two objects. Fig. 2a shows a possible relationship between polyhedra A and B as the result of derivation from the models of A and B and their sensed configurations. Clearly such a relationship is impossible in reality, whereas, based on this derived relationship, there is more than one contact situation that may actually occur due to uncertainties, as shown in Fig. 2b. Notice that an intrusion in the derived relationship, as it is caused by uncertainties, always means a possible contact, but absence of certain contacts in the derived relationship does not mean that those contacts cannot possibly occur in reality (e.g., see Fig. 2, where the point p of A may actually contact B as shown in Fig. 2b). Thus, it is quite difficult to determine the set of all possible contact situations between A and B taking into account location uncertainties.

The approach proposed in[24] simplified the problem by demanding the satisfaction of some geometric constraints, and thus was not completely general. On the other hand, the technique introduced in this paper, of growing objects by location uncertainties, fundamentally facilitates the finding of such a set in a general way. With the set serving as an initial guidance, as demonstrated in[4, 25, 20], additional sensing means, such as force/moment or vision sensing, can be used to reduce the set through confirming the existence (or non-existence) of each possible contact situation.

This approach of using different sensors to compensate for the uncertainties of one another is essential to accurate contact recognition, which in turn, is essential for task state recognition and for devising error recovery strategies as different contact situations may require different recovery motions[26, 5, 14, 9, 23].

The paper is organized as follows. In Section 2, we define a general uncertainty model in terms of position and orientation uncertainty bounds. In Section 3 and Section 4, we present how to grow a polyhedron by position and orientation uncertainties respectively, and in Section 5, we outline how to grow a polyhedron by location uncertainty, i.e., both position and orientation uncertainties. Based on the results in previous sections, we introduce three types of regions of a polyhedron in Section 6. In Section 7, we discuss how to apply the technique of growing a polyhedron to recognizing topological contacts. We conclude the paper in Section 8.

2 Uncertainty Model

We describe the configuration, i.e., the location L of a solid object as (M, \mathbf{p}) , where $\mathbf{p} \in \mathbf{R}^3$ denotes the position of the origin of the object frame in a world coordinate system and M is the rotation matrix of the object frame with respect to the world coordinate system, which describes the orientation of the object frame. We denote $\hat{L} = (\hat{M}, \hat{\mathbf{p}})$ as an *estimate* of $L = (M, \mathbf{p})$.

In the rest of the paper, we will use the subscripts $_p$ and $_o$ to indicate *position-related* and *orientation-related* parameters respectively.

Definition 1. The *position uncertainty* ϵ_p denotes the magnitude of the maximum possible difference between an estimated position $\hat{\mathbf{p}}$ and the actual one \mathbf{p} .

If we denote the Pythagorean metric on \mathbf{R}^3 as D_p , the set of all possible actual positions $N_p(\hat{\mathbf{p}})$ is the $D_p - \epsilon_p$ -neighborhood of $\hat{\mathbf{p}}$ (Fig. 3a). $N_p(\hat{\mathbf{p}})$ can be abbreviated as N_p .

Definition 2. For a solid object P , let \mathbf{q} denotes the position vector of the point $q \in P$ with respect to the origin of the object frame of P . The *orientation sensing uncertainty* ϵ_o denotes the magnitude of the maximum possible angle between the actual vector \mathbf{q} and its estimate $\hat{\mathbf{q}}$ for all points $q \in P$.

Let $\mathbf{M}_{3 \times 3}(R)$ be the set of rotational (orthogonal) matrices. From the fact that $\forall M_1, M_2 \in \mathbf{M}_{3 \times 3}(R), M_1 \neq M_2, \exists$ a unique axis of rotation \mathbf{a} and a unique angle $\gamma \in [-\pi, \pi]$, such that the rotation matrix $Rot(\mathbf{a}, \gamma)$ (about \mathbf{a} with angle γ) satisfies

$$Rot(\mathbf{a}, \gamma) = M_1^{-1} \cdot M_2 = M_1^T \cdot M_2,$$

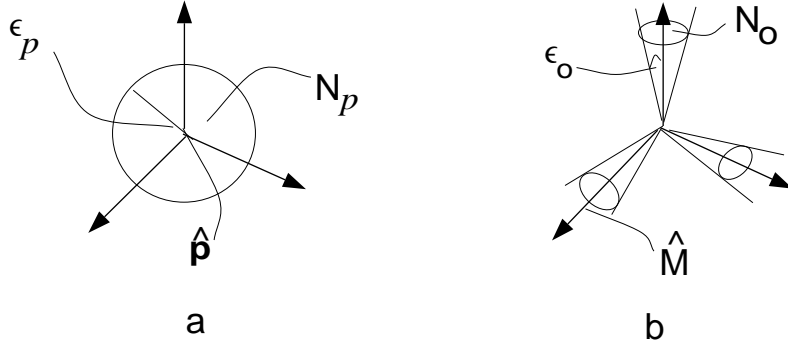


Figure 3: N_p and N_o

we can define a metric D_o on $\mathbf{M}_{3 \times 3}(R)$ such that $D_o(M_1, M_2) = |\gamma|$ (see Appendix A for a proof). Thus, the set of all possible actual orientations $N_o(\hat{M})$ is the D_o - ϵ_o -neighborhood of \hat{M} (Fig. 3b). $N_o(\hat{M})$ can be abbreviated as N_o .

The Cartesian product $N_p \times N_o$ describes the region of location uncertainty, i.e., the set of all possible locations under the estimated location \hat{L} due to position uncertainty ϵ_p and orientation uncertainty ϵ_o .

3 Growing a Polyhedron P by its Position Uncertainty

We first define the grown regions of a point, an edge, and a face of P respectively.

Definition 3. If the orientation of P is fixed, then for any point $q \in P$ or rigidly attached to P , any edge $e \in P$, and any face $f \in P$, the regions $\mathcal{Q}_p(\hat{\mathbf{p}})$, $\mathcal{E}_p(\hat{\mathbf{p}})$, and $\mathcal{F}_p(\hat{\mathbf{p}})$ defined as

$$\mathcal{Q}_p(\hat{\mathbf{p}}) = \bigcup_{\mathbf{p} \in N_p} q(\mathbf{p}) \quad \mathcal{E}_p(\hat{\mathbf{p}}) = \bigcup_{\mathbf{p} \in N_p} e(\mathbf{p}) \quad \mathcal{F}_p(\hat{\mathbf{p}}) = \bigcup_{\mathbf{p} \in N_p} f(\mathbf{p})$$

are the *grown regions of the point q , the edge e , and the face f by the position uncertainty of P* respectively, where $q(\mathbf{p})$, $e(\mathbf{p})$, and $f(\mathbf{p})$ denote the corresponding point, edge, and face which q , e , and f occupy when P is at position \mathbf{p} respectively. $\mathcal{Q}_p(\hat{\mathbf{p}})$, $\mathcal{E}_p(\hat{\mathbf{p}})$, and $\mathcal{F}_p(\hat{\mathbf{p}})$ can be abbreviated as \mathcal{Q}_p , \mathcal{E}_p , and \mathcal{F}_p respectively. If $q = v$, a vertex point of P , then \mathcal{Q}_p can also be denoted as \mathcal{V}_p .

It is rather easy to obtain these grown regions. We describe them in the following theorems.

Theorem 1. For any point $q \in P$ or rigidly attached to P , its grown region \mathcal{Q}_p by position uncertainty is the ball centered at $q(\hat{\mathbf{p}})$ with radius ϵ_p .

Proof. By the Definition 1 of position uncertainty in Section 2, N_p represents a ball centered at the origin O of the object frame of P in the world coordinate system, with radius ϵ_p . By the above Definition 3, that ball is the grown region of the point

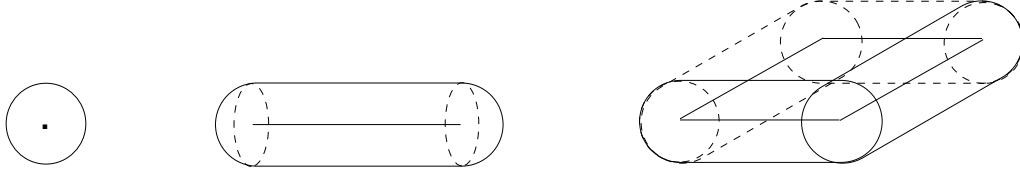


Figure 4: The grown regions \mathcal{V}_p , \mathcal{E}_p and \mathcal{F}_p

O by position uncertainty. Since q is rigidly attached to P , i.e., to point O , when O is at the position $\hat{\mathbf{p}}$, q is at the point $q(\hat{\mathbf{p}})$, and when O moves in the ball represented by N_p , q must move in a ball of the same size centered at $q(\hat{\mathbf{p}})$, which, by Definition 3, is the region \mathcal{Q}_p . \blacksquare

Theorem 2. The grown regions \mathcal{V}_p of a vertex $v \in P$, \mathcal{E}_p of an edge $e \in P$, and \mathcal{F}_p of a face $f \in P$ are as described below (Fig. 4).

- \mathcal{V}_p is the ball centered at $v(\hat{\mathbf{p}})$ with radius ϵ_p .
- \mathcal{E}_p consists of a cylinder of radius ϵ_p with axis being $e(\hat{\mathbf{p}})$ and two half balls of radius ϵ_p centered at the two end points of $e(\hat{\mathbf{p}})$ respectively.
- Let e^1, \dots, e^m denote the bounding edges of f and $\mathcal{E}_p^1, \dots, \mathcal{E}_p^m$ be their grown regions by position uncertainty respectively. Then, \mathcal{F}_p is a closed region formed by the union of $\mathcal{E}_p^1, \dots, \mathcal{E}_p^m$, and a right prism of height $2\epsilon_p$, which can be obtained by sweeping the planar surface $f(\hat{\mathbf{p}})$ along its normal directions up and down distance ϵ_p respectively.

Proof. The description of \mathcal{V}_p is based on Theorem 1. Since both an edge and a face are sets of points, their grown regions should be unions of the grown regions of the points in the edge and face sets respectively. Thus, \mathcal{E}_p can be viewed as the sweeping volume of the ball \mathcal{Q}_p as the center $q(\hat{\mathbf{p}})$ changes from one end point of $e(\hat{\mathbf{p}})$ to the other. \mathcal{F}_p can be viewed as the sweeping volume of the ball \mathcal{Q}_p as the center $q(\hat{\mathbf{p}})$ moves on the closed planar surface $f(\hat{\mathbf{p}})$. \blacksquare

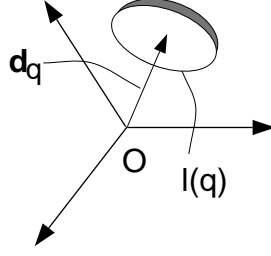


Figure 5: The grown region \mathcal{Q}_o of q

4 Growing a Polyhedron P by its Orientation Uncertainty

4.1 Growing a point q of P

Definition 4. For any point $q \in P$ or rigidly attached to P , if the position of P is fixed,

$$\mathcal{Q}_o(\hat{M}) = \bigcup_{M \in N_o(\hat{M})} q(M)$$

is the *grown region of the point q by orientation uncertainty of P* , where $q(M)$ denotes the corresponding point which q occupies when P is at orientation M . $\mathcal{Q}_o(\hat{M})$ can be abbreviated as \mathcal{Q}_o . If $q = v$, a vertex point of P , then \mathcal{Q}_o can also be written as \mathcal{V}_o .

Theorem 3. For any point $q \in P$ or rigidly attached to P , let $\mathbf{d}_q \neq 0$ denote the distance vector from the origin O of the object frame of P to q , measured with respect to the object frame of P . The grown region \mathcal{Q}_o of P by the orientation uncertainty of P is a spherical segment of one base as shown in Fig. 5, such that the sphere is centered at O with radius d_q , and \mathcal{Q}_o is bounded by the circle $l(q)$ centered at position $(\cos \epsilon_o)\mathbf{d}_q$ relative to the object frame of P and with radius $d_q \sin \epsilon_o$.

Proof. By Definition 4, \mathcal{Q}_o is defined under a fixed position of P , i.e., the origin O is unchanged. Thus, as the point q rigidly attaches to O , change of orientation of P only causes rotations of q about O . In other words, \mathcal{Q}_o is a region on the sphere centered at O with the radius being $d_q = \|\mathbf{d}_q\|$. Furthermore, if $\mathbf{d}_q(M)$ denotes the distance vector from the origin O to the point $q(M)$, by Definition 2 of orientation uncertainty, $\mathbf{d}_q(M)$ must be inside the uncertainty cone whose axis coincides with the vector $\mathbf{d}_q(\hat{M})$ as shown in Fig. 6a, for all $M \in N_o$. Thus, the region \mathcal{Q} is the intersection of the sphere and the cone, which is a spherical segment of one base (Fig. 6a). In addition, for any orientation M of P , the following holds: $\|\mathbf{d}_q(M)\| = d_q$, and if represented with

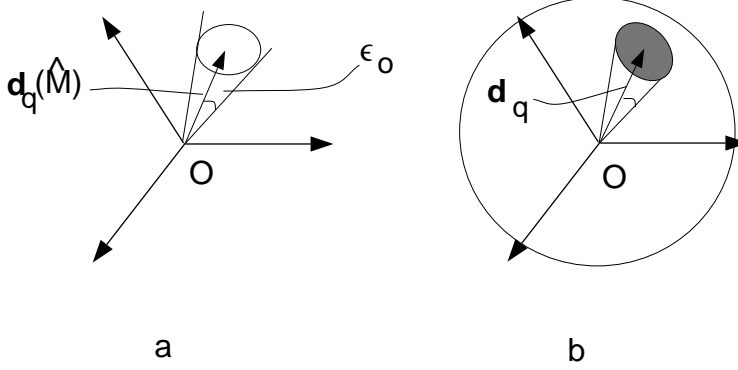


Figure 6: The formation of surface \mathcal{Q}_o of q

respect to the object frame of P , $\mathbf{d}_q(M) = \mathbf{d}_q$. Thus, as illustrated in Fig. 6b, the bounding circle $l(q)$ is centered at $(\cos \epsilon_o)\mathbf{d}_q$ with radius $d_q \sin \epsilon_o$. \blacksquare

4.2 Growing an edge e of P

Definition 5. For any edge $e \in P$, if the position of P is fixed,

$$\mathcal{E}_o(\hat{M}) = \bigcup_{M \in N_o(\hat{M})} \epsilon(M)$$

is the *grown region of the edge e by the orientation uncertainty of P* , where $\epsilon(M)$ denotes the corresponding line segment which e occupies when P is at orientation M . $\mathcal{E}_o(\hat{M})$ can be abbreviated as \mathcal{E}_o .

Since an edge consists of points, for an edge $e \in P$, apparently,

$$\mathcal{E}_o(\hat{M}) = \bigcup_{q \in e} \mathcal{Q}_o(\hat{M}).$$

Since by Theorem 3, the shape and size of $\mathcal{Q}_o, \forall q \in e$, depends on the spatial relationship between the point q and the origin O of the object frame of P , it is clear that the shape and size of \mathcal{E}_o depends on the spatial relationship between the edge e and the origin O (the center of rotation). For convenience, we set up a coordinate system $o - xyz$ at O in such a way that e is parallel to the z axis and on the xz plane with x being positive, β_1 and β_2 denote the angles between positive z axis and the two end-point position vectors of e respectively with $\beta_1 < \beta_2$, and d_e denote the distance between the line which contains e and the z axis. Now, one can classify the spatial relationships between e and O into the following classes:

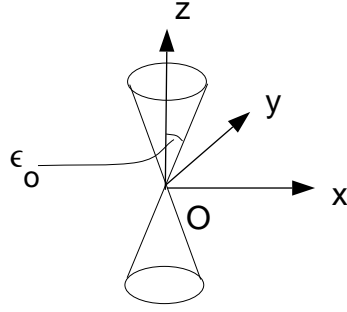


Figure 7: \mathcal{E}_o is part of the cone if e is on z

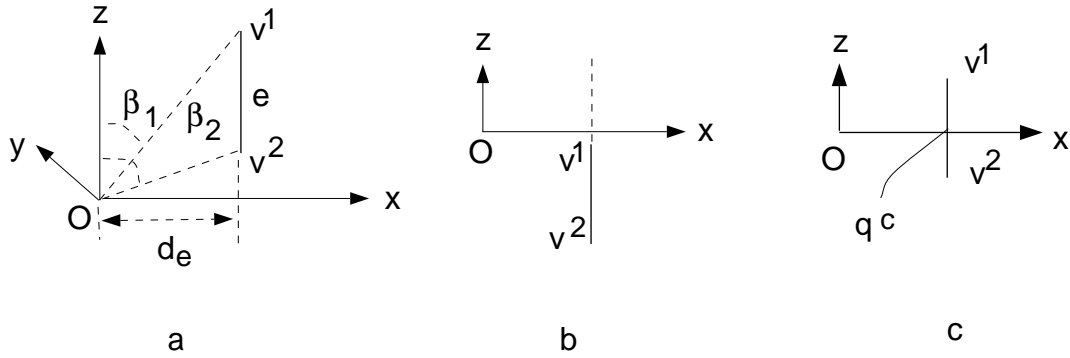


Figure 8: e is not on z , and \mathcal{E}_o does not intersect z

1. e is on z ;
2. e is not on z :
 - (a) \mathcal{E}_o intersects z ;
 - (b) \mathcal{E}_o does not intersect z .

For cases in the first class, \mathcal{E}_o is simply part of the circular (uncertainty) cone as shown in Fig. 7, bounded by the grown surfaces \mathcal{V}_o^1 and \mathcal{V}_o^2 of the end vertices of e .

For cases in the second class, however, \mathcal{E}_o is not a circular cone and is difficult to describe in terms independent of coordinates. For each case, the analytical equations describing \mathcal{E}_o , can be derived; but for different cases, the descriptions are slightly different. For the sake of brevity, we only present how to derive the analytical descriptions of \mathcal{E}_o for the cases described by class 2(b) above, also as shown in Fig. 8, in the following Theorems 4 to 6. The descriptions of \mathcal{E}_o for other cases can be derived in a similar way.

Theorem 4. Give an edge $e \in P$ satisfying the spatial relationship with a coordinate system $o-xyz$ as shown in Fig. 8a, where the origin O is the center of rotation, v^1 and

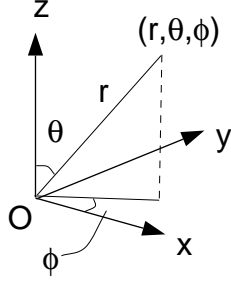


Figure 9: The spherical coordinate system

v^2 are end vertices, and $\beta_1 < \beta_2 \leq \pi/2$. The grown region \mathcal{E}_o of e by the orientation uncertainty of P has a boundary surface formed by the grown surface \mathcal{V}_o^1 of v^1 , the grown surface \mathcal{V}_o^2 of v^2 , and the surface \mathcal{E}_s which consists of points on the boundary circle $l(q)$ of \mathcal{Q}_o for all $q \in e$. \mathcal{E}_s is described by the following equation in the spherical coordinate system (r, θ, ϕ) established as shown in Fig. 9:

$$\cos \phi = \frac{r \cos \epsilon_o - \cos \theta \sqrt{r^2 - d_e^2}}{d_e \sin \theta}, \quad (1)$$

where

$$\begin{cases} \frac{d_e}{\sin \beta_2} \leq r \leq \frac{d_e}{\sin \beta_1} \\ \beta_1 - \epsilon_o \leq \theta \leq \beta_2 + \epsilon_o \end{cases} \quad (2)$$

Proof. We first use a parameter β , defined as the angle between the positive z axis and the position vector of the point considered, to describe a point on e such that for any point $q \in e$, its spherical coordinates are expressed as $(d_e / \sin \beta, \beta, 0)$ (Fig. 10). Thus, q can be denoted as a function of β : $q(\beta)$, where $\beta \in [\beta_1, \beta_2]$. Obviously $q(\beta)$ is a one-to-one function of β . Thus, the grown surface \mathcal{Q}_o of q , as defined in Theorem 3, can be uniquely identified as $\mathcal{Q}_o(\beta)$; for any point $s \in \mathcal{Q}_o(\beta)$, its r coordinate satisfies

$$r = \frac{d_e}{\sin \beta}, \quad (3)$$

and its θ coordinate satisfies

$$\theta = \beta + \alpha, \quad (4)$$

where $\alpha \in [-\epsilon_o, \epsilon_o]$. Appendix B shows that $l(q)$, the boundary circle of $\mathcal{Q}_o(\beta)$, satisfies

$$\begin{cases} \cos \phi = \frac{r \cos \epsilon_o - \cos \theta \sqrt{r^2 - d_e^2}}{d_e \sin \theta} \\ r = \frac{d_e}{\sin \beta} \end{cases} \quad (5)$$

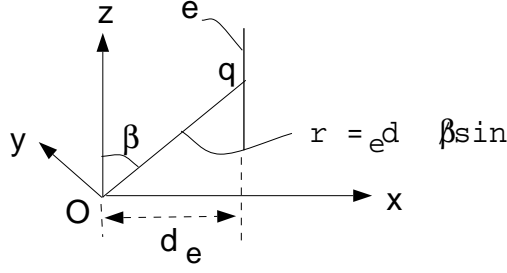


Figure 10: e described by parameter β

Since \mathcal{E}_o is the union of $\mathcal{Q}_o(\beta)$ for all $\beta \in [\beta_1, \beta_2]$, the equations (3) and (4) in fact describe every point (r, θ, ϕ) in \mathcal{E}_o , provided that $\beta \in [\beta_1, \beta_2]$, $\alpha \in [-\epsilon_o, \epsilon_o]$, and ϕ is within the boundary defined by (5):

$$\cos \phi \geq \frac{r \cos \epsilon_o - \cos \theta \sqrt{r^2 - d_e^2}}{d_e \sin \theta}. \quad (6)$$

We next try to determine the bounds on r and θ . From equation (3) and the fact that $[\beta_1, \beta_2] \subset (0, \pi/2]$, r is a monotonically decreasing function of β for $\beta \in [\beta_1, \beta_2]$. Thus, r assumes upper and lower bounds at $\beta = \beta_1$ and $\beta = \beta_2$ respectively, that is,

$$\frac{d_e}{\sin \beta_2} \leq r \leq \frac{d_e}{\sin \beta_1}. \quad (7)$$

As for θ , from (4), it is obvious that θ assumes upper and lower bounds when β and α assume their upper and lower bounds respectively, that is,

$$\beta_1 - \epsilon_o \leq \theta \leq \beta_2 + \epsilon_o. \quad (8)$$

The boundary surface of \mathcal{E}_o contains points where any of the coordinates among r , θ , and ϕ assumes bounding values as described in (7), (8), and (6) respectively. Since $\mathcal{Q}_o(\beta_1)$ and $\mathcal{Q}_o(\beta_2)$ are surfaces where r assumes the upper bound and lower bound values respectively, the two surfaces, which are also denoted as \mathcal{V}_o^1 and \mathcal{V}_o^2 , are part of the boundary surface of \mathcal{E}_o . Having ϕ take its bound values is equivalent to changing (6) to an equation, which is exactly the equation (1). Thus, the surface \mathcal{E}_s is described by (1), which consists of the points on the boundary circle $l(q)$ of \mathcal{Q}_o for all $q \in e$. ■

Fig. 11 illustrates the surface \mathcal{E}_o described in Theorem 4.

Theorem 5. Give an edge $e \in P$ satisfying the spatial relationship with a coordinate system $o - xyz$ as shown in Fig. 8b, where the origin O is the center of rotation, v^1 and v^2 are end vertices, and $\pi/2 \leq \beta_1 < \beta_2$. The grown region \mathcal{E}_o of e has a boundary surface consisting of the grown surface \mathcal{V}_o^1 of v^1 , the grown surface \mathcal{V}_o^2 of v^2 , and the

surface \mathcal{E}_s which consists of points on the boundary circle $l(q)$ of \mathcal{Q}_o for all $q \in e$. \mathcal{E}_s is described by the following equation in the spherical coordinate system (r, θ, ϕ) established as shown in Fig. 9:

$$\cos \phi = \frac{r \cos \epsilon_o + \cos \theta \sqrt{r^2 - d_e^2}}{d_e \sin \theta}, \quad (9)$$

where

$$\begin{cases} \frac{d_e}{\sin \beta_1} \leq r \leq \frac{d_e}{\sin \beta_2} \\ \beta_1 - \epsilon_o \leq \theta \leq \beta_2 + \epsilon_o \end{cases} \quad (10)$$

Proof. The proof is almost identical to that of Theorem 4. Noticing that here $\beta \geq \pi/2$, (9) can also be derived following Appendix B. \blacksquare

Fig. 12 illustrates the surface \mathcal{E}_o described in Theorem 5.

Theorem 6. Give an edge $e \in P$ satisfying the spatial relationship with a coordinate system $o - xyz$ as shown in Fig. 8c, where the origin O is the center of rotation, $\beta_1 < \pi/2$, and $\beta_2 > \pi/2$. The grown region \mathcal{E}_o of e has a boundary surface consisting of the two grown surfaces \mathcal{V}_o^1 and \mathcal{V}_o^2 of the end vertices v^1 and v^2 respectively, the grown surface \mathcal{Q}_o^c of q^c (the closest point on e to O), and the surface \mathcal{E}_s , described by the following equation in the spherical coordinate system (r, θ, ϕ) established as shown in Fig. 9:

$$\cos \phi = \begin{cases} \frac{r \cos \epsilon_o - \cos \theta \sqrt{r^2 - d_e^2}}{d_e \sin \theta}, & \text{if } \theta \leq \pi/2 \\ \frac{r \cos \epsilon_o + \cos \theta \sqrt{r^2 - d_e^2}}{d_e \sin \theta}, & \text{otherwise} \end{cases} \quad (11)$$

where

$$\begin{cases} d_e \leq r \leq \frac{d_e}{\min(\sin \beta_1, \sin \beta_2)} \\ \beta_1 - \epsilon_o \leq \theta \leq \beta_2 + \epsilon_o \end{cases} \quad (12)$$

Proof. As in the proof for Theorem 4, the same parameters β and α are used to express r and θ as in (3) and (4) respectively. However, here r is not a monotonical function of β for $\beta \in [\beta_1, \beta_2]$. Instead, r reaches the minimum value d_e at $\beta = \pi/2$, which corresponds to the grown surface \mathcal{Q}_o^c of q^c , the closest point on e to O (see Fig. 8c). Thus, \mathcal{Q}_o^c is also part of \mathcal{E}_o , and the bounds on r are as shown in (12), which are different from those in the case of Theorem 4. The rest of the proof follows exactly as that of Theorem 4. Equation (11) can also be derived following Appendix B. \blacksquare

Note that the situation described in Theorem 6 (shown in Fig. 8c) can be viewed as the combination of the two situations shown in Fig. 8a and b: one with $\beta_1 < \beta_2 = \pi/2$ and the other with $\pi/2 = \beta_1 < \beta_2$. Thus, the grown region \mathcal{E}_o can also be obtained by applying Theorems 4 and 5 to the two situations respectively; the combined result is the same as described in Theorem 6.

Fig. 13 illustrates the surface \mathcal{E}_o described in Theorem 6.

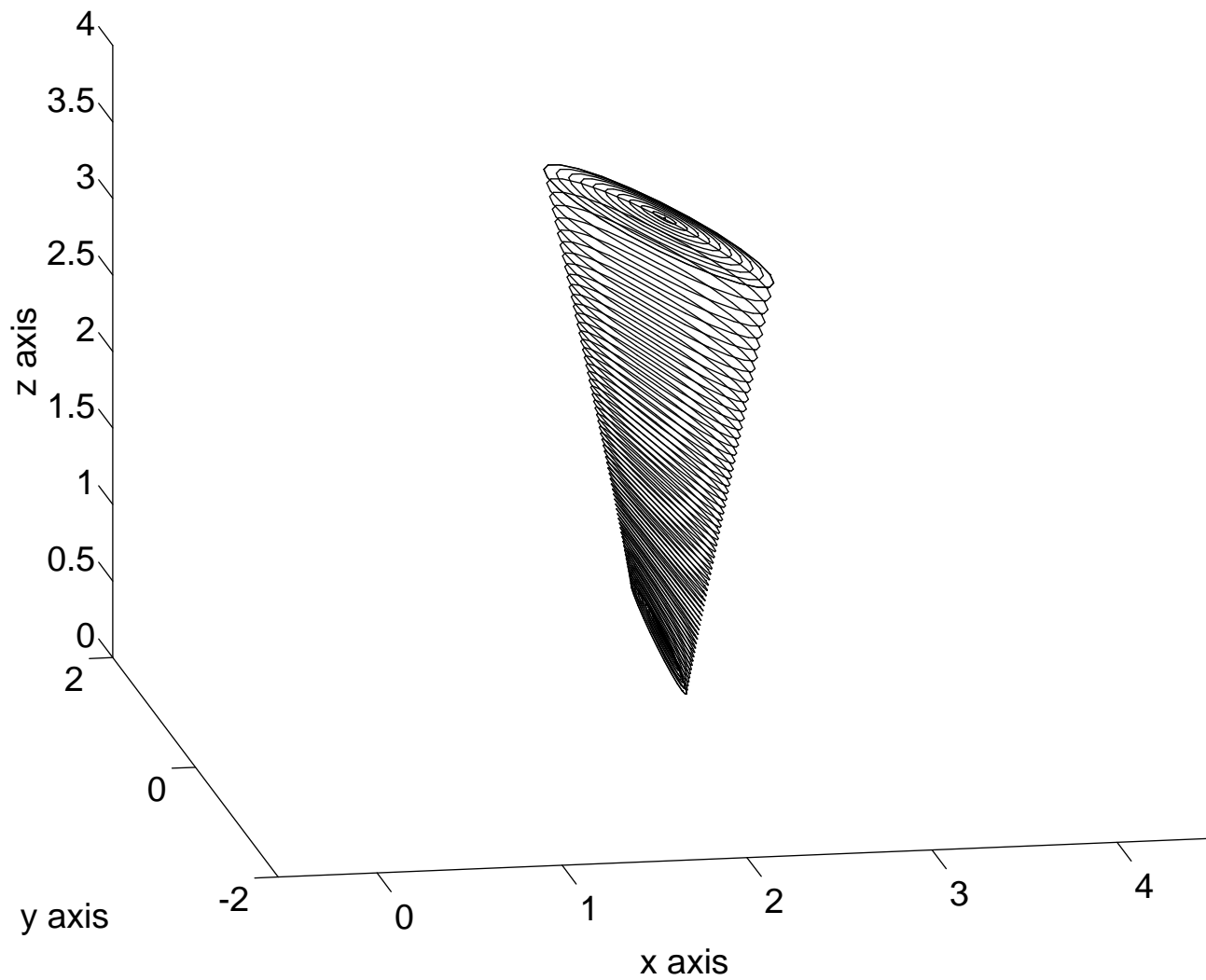


Figure 11: The surface \mathcal{E}_o described in Theorem 4

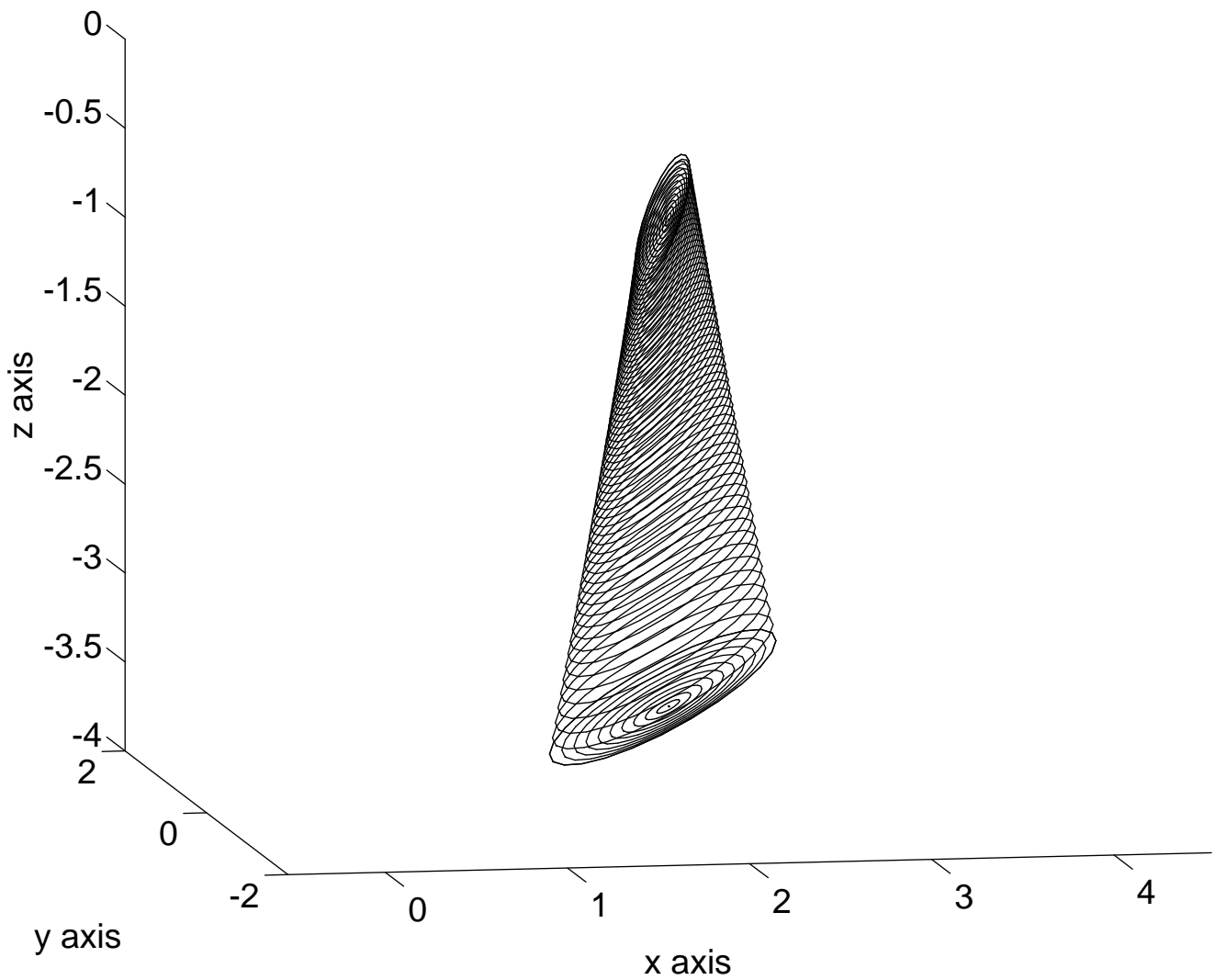


Figure 12: The surface \mathcal{E}_o described in Theorem 5

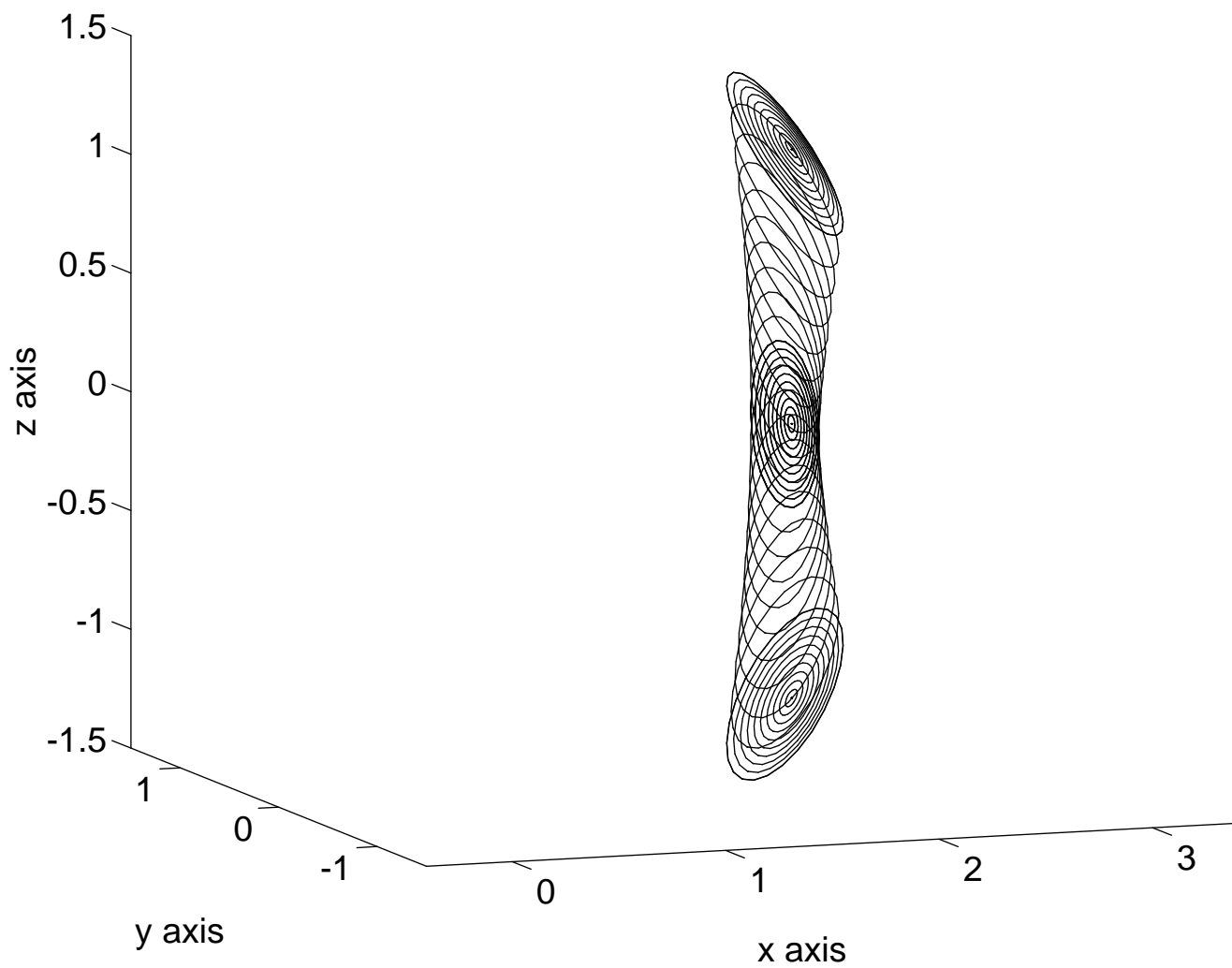


Figure 13: The surface \mathcal{E}_0 described in Theorem 6

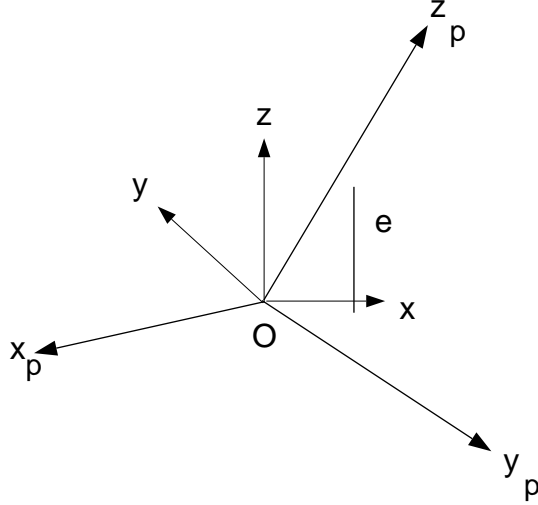


Figure 14: \mathcal{E}_o w.r.t. the frame of P can be obtained by coordinate transforms

The general description of \mathcal{E}_o with respect to the object frame of P can be obtained easily through the transform from the spherical coordinates to the Cartesian coordinates and then the rotational transform from $o - xyz$ to the object frame $o - x_p y_p z_p$ of P (Fig. 14).

4.3 Growing a plane a containing a face f of P

Definition 6. For a plane a which contains a face $f \in P$ and therefore rigidly attached to P , if the position of P is fixed,

$$\mathcal{A}_o(\hat{M}) = \bigcup_{M \in N_o(\hat{M})} a(M)$$

is the *grown region of the plane a by the orientation uncertainty of P* , where $a(M)$ denotes the corresponding plane which a occupies when P is at orientation M . $\mathcal{A}_o(\hat{M})$ can be abbreviated as \mathcal{A}_o .

Theorem 7. For a plane a which contains a face $f \in P$ and therefore rigidly attached to P , the boundary surface of the grown region $\mathcal{A}_o(\hat{M})$ of a consists of two surfaces \mathcal{A}_{far} and \mathcal{A}_{near} , such that

1. if O is on a , \mathcal{A}_{far} and \mathcal{A}_{near} are the boundary surfaces of the two nappes of the circular cone with angle being $(\pi/2 - \epsilon_o)$ whose apex is at O (Fig. 15a);
2. if O is not on a and \mathbf{d} denotes the distance vector from O to the closest point $d \in a$, and \mathcal{K} denotes the circular cone with angle being $(\pi/2 - \epsilon_o)$ whose apex is at position $\mathbf{d}/\cos \epsilon_o$, then \mathcal{A}_{far} is the boundary surface of the nappe of \mathcal{K} further from O along \mathbf{d} , and \mathcal{A}_{near} consists of the boundary surface of the other nappe and the grown surface \mathcal{D}_o of the point d as described in Theorem 4 (Fig. 15b).

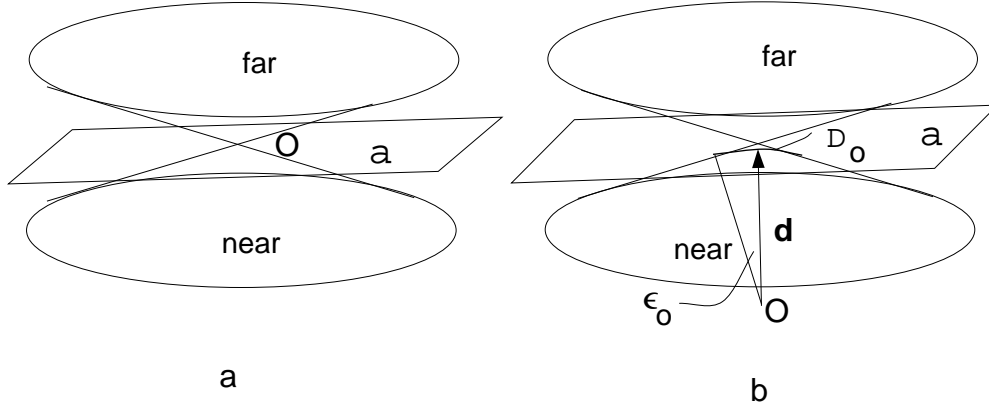


Figure 15: The surface of \mathcal{A}_o

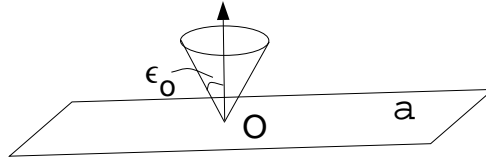


Figure 16: The normal vector \mathbf{n} of a

Proof. First, let us focus on the case where O is on a . Consider a unit normal vector \mathbf{n} of a originated from O . \mathbf{n} is rigidly attached to a , and thus to P . By Definition 2, when P is at all orientations in N_o , the vector \mathbf{n} is within the orientation uncertainty cone of angle ϵ_o with vertex at O (Fig. 16). When \mathbf{n} sweeps the boundary surface of the cone, the plane a , always perpendicular to \mathbf{n} , sweeps the boundary surface of \mathcal{A}_o accordingly, which is the surface of the circular cone as stated in the theorem (Fig. 15a).

In the case where O is not on a , the position vector \mathbf{d} of d is a normal vector of a . When P is at all orientations in N_o , by Definition 2, \mathbf{d} is within the orientation uncertainty cone of angle ϵ_o with vertex at O , and by Theorem 3, the point d is on a spherical surface \mathcal{D}_o with the boundary circle $l(d)$. When \mathbf{d} sweeps the boundary of the cone, i.e., when d sweeps the circle $l(d)$, the plane a , always perpendicular to \mathbf{d} , sweeps the boundary surface of \mathcal{A}_o accordingly, which is the surface as stated in the theorem (Fig. 15b). ■

4.4 Growing a face f of P

Definition 7. For any face $f \in P$ if the position of P is fixed,

$$\mathcal{F}_o(\hat{M}) = \bigcup_{M \in N_o(\hat{M})} f(M)$$

is the *grown region of the face f by the orientation uncertainty of P* , where $f(M)$ denotes the corresponding planar surface which f occupies when P is at orientation M . $\mathcal{F}_o(\hat{M})$ can be abbreviated as \mathcal{F}_o .

Theorem 8. For any (planar) face $f \in P$, which is bounded by e^1, e^2, \dots, e^m edges, where $m \geq 3$, the grown region \mathcal{F}_o of f is a closed region obtained by the union of the grown regions $\mathcal{E}_o^1, \mathcal{E}_o^2, \dots, \mathcal{E}_o^m$, and the part of the grown region \mathcal{A}_o of the plane a containing f which is bounded by $\mathcal{E}_o^1, \mathcal{E}_o^2, \dots, \mathcal{E}_o^m$.

Proof. Because the planar face f is a closed set that is the part of the plane a bounded by the edges e^1, e^2, \dots, e^m , by Definitions 6 and 7, the grown region \mathcal{F}_o of f is also a closed set that is the part of the grown region of a bounded by the grown regions of the edges of f . \blacksquare

5 Growing A Polyhedron P by Both Position and Orientation Uncertainties

We first define the grown regions of a point, an edge, and a face of P by location uncertainty, consisting of both position and orientation uncertainties.

Definition 8. For any point $q \in P$ or rigidly attached to P , any edge $e \in P$, and any face $f \in P$, the regions $\mathcal{Q}(\hat{L})$, $\mathcal{E}(\hat{L})$, and $\mathcal{F}(\hat{L})$, defined as

$$\mathcal{Q}(\hat{L}) = \bigcup_{L \in N_p \times N_o} q(L) \quad \mathcal{E}(\hat{L}) = \bigcup_{L \in N_p \times N_o} e(L) \quad \mathcal{F}(\hat{L}) = \bigcup_{L \in N_p \times N_o} f(L)$$

are the *grown regions of the point q , the edge e , and the face f by the location uncertainty of P* respectively, where $q(L)$, $e(L)$, and $f(L)$ denote the corresponding point, edge and face which q , e , and f occupy respectively when P is at location L . $\mathcal{Q}(\hat{L})$, $\mathcal{E}(\hat{L})$, $\mathcal{F}(\hat{L})$ can be abbreviated as \mathcal{Q} , \mathcal{E} , and \mathcal{F} respectively. If $q = v$, a vertex point of P , then \mathcal{Q} can also be denoted as \mathcal{V} .

Given a point q , an edge e , or a face f of a polyhedron P , whose estimated location is $\hat{L} = (\hat{\mathbf{p}}, \hat{M})$, to obtain \mathcal{V} , \mathcal{E} , and \mathcal{F} , we can first obtain the grown region $\mathcal{Q}_o(\hat{\mathbf{p}})$ of q , $\mathcal{E}_o(\hat{\mathbf{p}})$ of e , or $\mathcal{F}_o(\hat{\mathbf{p}})$ of f (Section 4), and then grow the obtained \mathcal{V}_o , \mathcal{E}_o , or \mathcal{F}_o by position uncertainty ϵ_p .

Note that since \mathcal{V}_o , \mathcal{E}_o , and \mathcal{F}_o are not polyhedral, Section 3 cannot be readily applied to growing them by position uncertainty. However, growing a region by position uncertainty is not difficult to achieve in the first place: by “rolling” the position uncertainty ball along the boundary surface of the region, in our case, the

boundary surface of a \mathcal{V}_o , \mathcal{E}_o , or \mathcal{F}_o , with the center of the ball on the surface, the boundary surface swept is the boundary surface of the grown region \mathcal{V} , \mathcal{E} , or \mathcal{F} .

Specifically, the grown region \mathcal{Q} can be obtained by translating the surface \mathcal{Q}_o (described in Theorem 3) up and down a distance ϵ_p and filling the gap between two translated images of \mathcal{Q}_o by “rolling” the position uncertainty ball along the boundary curve of \mathcal{Q}_o with the center of the ball on the curve. The description of the grown region \mathcal{E} of an edge can be obtained based on the grown region \mathcal{Q} of a point by similar derivations as those in Section 4.2. The grown region \mathcal{A} of a plane a containing a face $f \in P$ by both position and orientation uncertainties can be obtained by translating the surface \mathcal{A}_{near} of $\mathcal{A}_o(\hat{\mathbf{p}})$ (see Section 4.3) towards the center of rotation O a distance ϵ_p and the surface \mathcal{A}_{far} away from O a distance ϵ_p . Finally, the grown region \mathcal{F} of the face f can be described based on \mathcal{A} and the grown regions \mathcal{E} ’s of the bounding edges of f in the similar way as described in Theorem 8.

6 Grown Regions, Grown Shell Regions, and Core Regions of a Polyhedron

Given the grown regions of individual faces of a polyhedron P : \mathcal{F}_p ’s, \mathcal{F}_o ’s, and \mathcal{F} ’s, as the results from Sections 3, 4, and 5 respectively, we can describe three types of uncertainty-related regions for the polyhedron P itself: the *grown regions* of P , the *grown shell regions* of P , and the *core regions* of P as the following.

Definition 9. For a polyhedron P ,

- its *grown regions* \mathcal{G}_p by position uncertainty, \mathcal{G}_o by orientation uncertainty, and \mathcal{G} by location uncertainty are the closed regions bounded by the union of \mathcal{F}_p ’s, the union of \mathcal{F}_o ’s, and the union of \mathcal{F} ’s respectively, of the faces of P ;
- its *grown shell regions* \mathcal{S}_p by position uncertainty, \mathcal{S}_o by orientation uncertainty, and \mathcal{S} by location uncertainty are the union of \mathcal{F}_p ’s, the union of \mathcal{F}_o ’s, and the union of \mathcal{F} ’s respectively, of the faces of P ;
- its *core regions* \mathcal{C}_p by position uncertainty, \mathcal{C}_o by orientation uncertainty, and \mathcal{C} by location uncertainty are the set differences $\mathcal{G}_p - \mathcal{S}_p$, $\mathcal{G}_o - \mathcal{S}_o$, and $\mathcal{G} - \mathcal{S}$ respectively.

The meanings of these regions are given in the following theorem.

Theorem 9. \mathcal{G}_p , \mathcal{G}_o , and \mathcal{G} are the uncertain regions possibly occupied by P under position, orientation, and location (i.e. both position and orientation) uncertainties respectively. \mathcal{S}_p , \mathcal{S}_o , and \mathcal{S} are the uncertain regions possibly occupied by the boundary surface of P under position, orientation, and location uncertainties respectively. \mathcal{C}_p , \mathcal{C}_o , and \mathcal{C} are the regions definitely occupied by P regardless of position uncertainty, orientation uncertainty, and location uncertainty respectively.

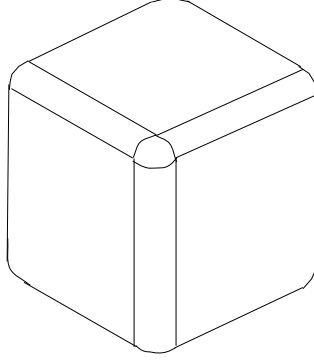


Figure 17: Illustration of the grown region \mathbf{G}_p of a cube

Proof. The interpretations of the grown regions and the grown shell regions are quite obvious so that we only focus on those of the core regions below. By Definition 9, the core region \mathcal{C}_p is the region enclosed by the region \mathcal{S}_p . For a fixed orientation of P , let $P(\mathbf{p})$ denote the region which P occupies at position \mathbf{p} . Since $\forall \mathbf{p} \in N_p$, the boundary surface of $P(\mathbf{p})$ is contained in \mathcal{S}_p , thus $P(\mathbf{p}) \supset \mathcal{C}_p$. Similarly, for a fixed position of P , let $P(M)$ denote the region which P occupies at orientation M , and we can show that $\forall M \in N_o, P(M) \supset \mathcal{C}_o$. Furthermore, let $P(L)$ denote the region which P occupies at location L , and we can show that $\forall L \in N_p \times N_o, P(L) \supset \mathcal{C}$. ■

Note that when uncertainties are too large, the core regions can become empty. Specifically, when the position uncertainty ϵ_p is so large that the family of grown regions of the (boundary) faces of P becomes a cover of P at $\hat{\mathbf{p}}$, then $\mathcal{G}_p = \mathcal{S}_p$, and $\mathcal{C}_p = \emptyset$. That is, no region is guaranteed to be occupied by P . Similar phenomenon can occur to core regions \mathcal{C}_o and \mathcal{C} .

Fig. 17, Fig. 18, and Fig 19 illustrate the grown regions \mathcal{G}_p , \mathcal{G}_o , and \mathcal{G} respectively of a cube whose object frame is established at its center.

7 Application to Contact Recognition

7.1 Contact Model

A contact situation between two polyhedra can be described in terms of the topological contacts among their surface elements, i.e., faces, edges, and vertices.

Definition 10. A *principal contact* (PC) is the single contact between a pair of topological surface elements from different objects which are not the boundaries of other contacting topological elements (if there is more than one pair in contact).

For example, the upper leftmost picture in Fig. 20 shows a PC of face-face (f-f) and not of edge-face or face-edge (f-e or e-f) or other types. Theoretically, there are

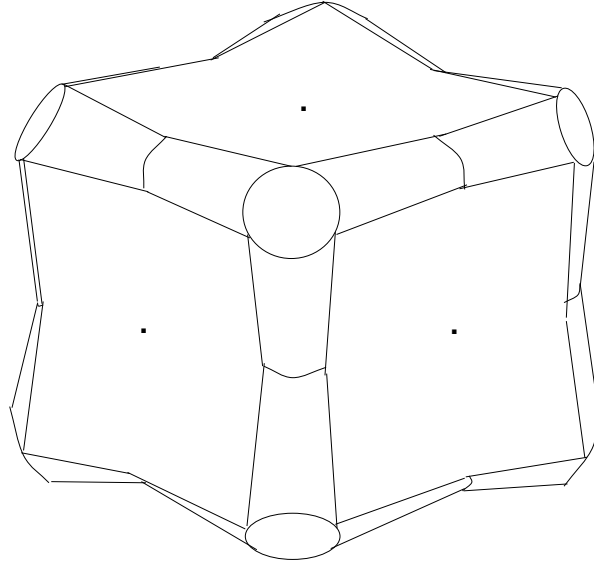


Figure 18: Illustration of the grown region \mathcal{G}_o for a cube with its frame set at center

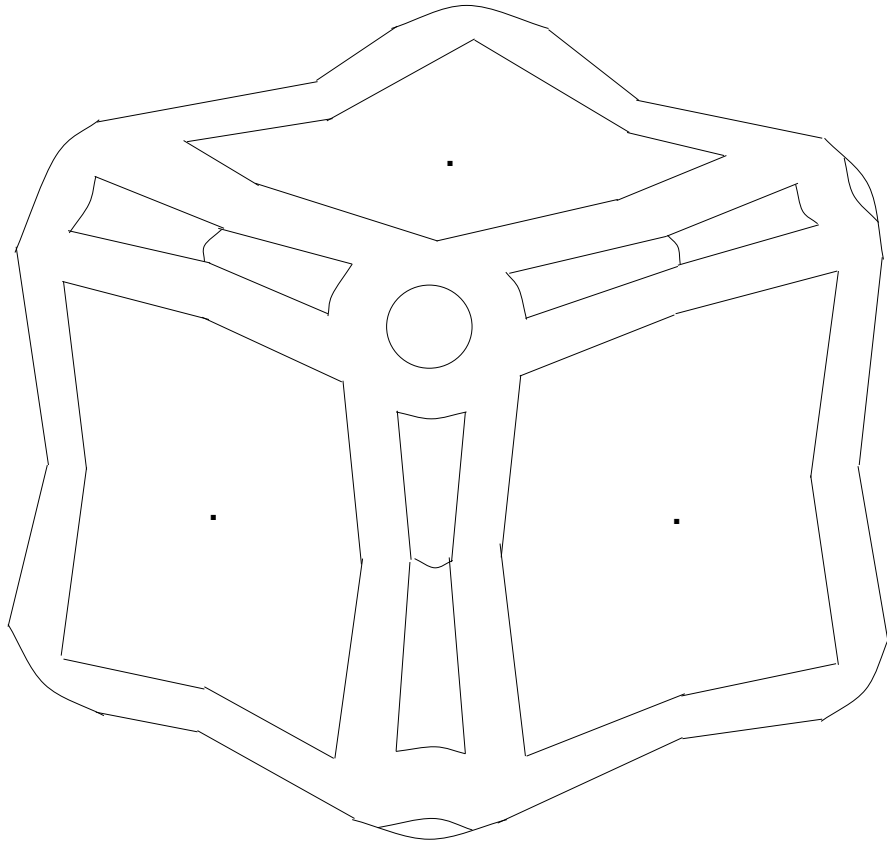


Figure 19: Illustration of the grown region \mathcal{G} for a cube with its frame set at center

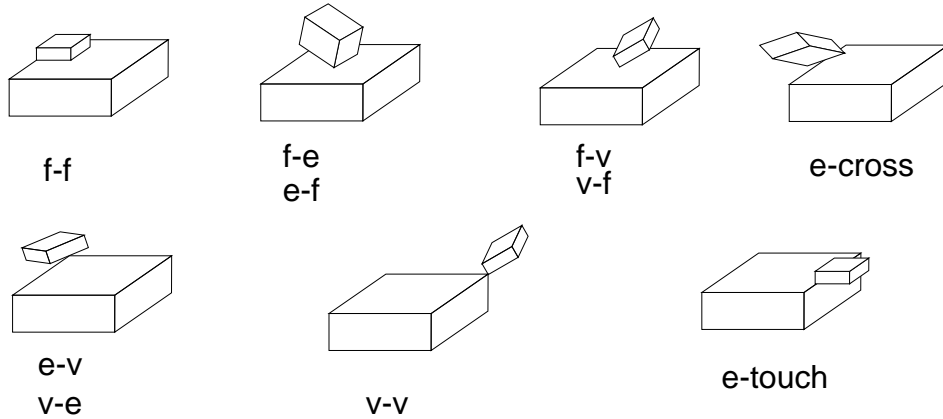


Figure 20: Principal contacts

ten types of possible PC's as shown in Fig. 20.

Definition 11. A *contact formation* (CF) represents a contact situation as the set of principal contacts formed (e.g., $\{ \langle f_1^1, f_3^2 \rangle, \langle e_4^1, f_1^2 \rangle, \dots \}$).

Note that the concept of CF is mostly aimed at describing a contact situation between two *nonconvex* objects. For two convex objects in contact, the CF should contain only a single PC.

7.2 Approach

Based on the contact model defined, the problem of contact recognition (as introduced in Section 1) can be formulated as: *given two polyhedral objects P_1 and P_2 in collision, their geometric models, and their estimated locations, find the contact formation between them taking into account location uncertainties.*

First, we can apply the technique of growing polyhedra by their location uncertainties to obtaining the set of all possible (due to uncertainties) principal contacts between P_1 and P_2 . We denote such a set as \mathcal{S}_{pc} .

Since contacts only occur between the boundary surfaces of two objects, all possible contacts between P_1 and P_2 due to uncertainties manifest to intersections between their grown shell regions only. As the result, we can analyze the intersection between the grown regions of one pair of surface elements (u_1, u_2) at a time, where u_1 (or u_2) is either a face, an edge, or a vertex of P_1 (or P_2), and continue the process until all pairs of such intersecting regions are considered. We certainly can also consider all such pairs of grown regions in parallel with a parallel processor. In any case, the task then is simplified to that of finding a mapping from the intersection between the two grown regions of u_1 and u_2 to whether or not the principal contact $\langle u_1, u_2 \rangle$ possibly exist. The implementation of such a task is described in the following subsection.

Once the set \mathcal{S}_{pc} is obtained, other sensing means can be used to reduce the set. Specifically, vision and/or force/moment sensing data can be used to verify if a PC

in S_{pc} actually exists or not [25, 4]. The vision and force/moment sensing can expect to eliminate non-existing PC's and to reduce S_{pc} , in the most desirable case, to a valid contact formation. Such contact formation shall represent the actual contact situation between P_1 and P_2 .

7.3 Implementation

Although from Sections 3, 4, and 5, we can describe analytically the grown regions of two surface elements, since the grown regions are nonpolyhedral and nonconvex, how to compute the kind of intersection between two such regions efficiently poses a great challenge. Nevertheless, since we aim at real-time recognition of contacts, to be computationally efficient is necessary.

Our practical solution at present includes the following two approximations:

1. approximate the precisely grown regions by circumscribing regions of simpler shapes,
2. instead of reasoning about the *kind* of intersection between two regions, simply check if the two regions intersect, and then use additional constraints to determine if a PC possibly exists.

The first approximation will not miss possible PC's but may introduce more PC's than the actually possible ones since if two precisely grown regions intersect, the regions circumscribing them also intersect, but *not* vice versa. The second approximation may also result in extra PC's than actually possible. For example, to decide if e_1 and e_2 in Fig. 21a can possibly be an e-touch principal contact (see Fig. 20), we may just check

- if the grown regions of e_1 and e_2 intersect, and
- if the angle between the original e_1 and e_2 is less than or equal to ϵ_o .

These conditions, however, are necessary but not sufficient, as evident from observing Fig. 21b, which shows a case that satisfies both conditions but does not suggest that e_1 and e_2 possibly form an e-touch PC. Hence, with both approximations, an upper bound of S_{pc} may be obtained. This, after all, is not too intolerable.

Specifically, we have implemented an algorithm [27] which approximates the precisely grown regions by regions built from S-topes [22, 10]. The approximation preserves major concavities of the grown regions. Given two polyhedral objects P_1 and P_2 in contact, the algorithm assumes that one of the objects, say, P_1 , is fixed, and that only P_2 has location uncertainty. Thus the problem becomes that of growing P_1 by the position uncertainty of P_2 and growing P_2 by its own orientation uncertainty only¹ (see Appendix C for a proof). By checking the intersection between every pair

¹Note that the algorithm should work equally well even if both P_1 and P_2 have location uncertainties since it is equally easy to approximate the grown regions by both position and orientation uncertainties with the S-tope model.

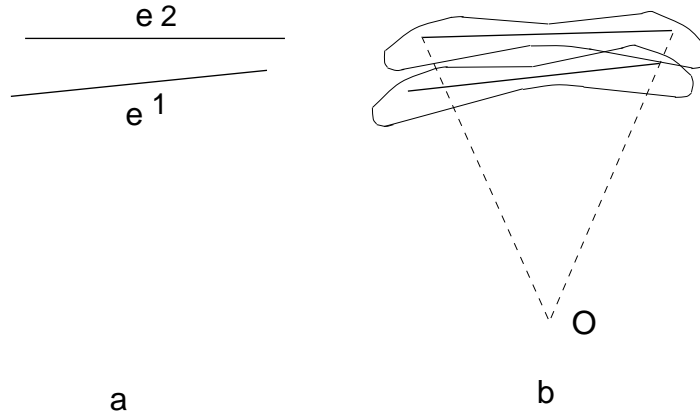


Figure 21: Determining if the PC $\langle e_1, e_2 \rangle$ possibly exists

of (approximated) grown regions of elements from the two objects respectively and with proper reasoning, the algorithm efficiently generates a set of PC's slightly larger than S_{pc} . As an example, for the two contacting objects A and B shown in Fig. 2, the algorithm spent 0.572 seconds of CPU time on a SUN SPARC IPX to generate an output set of PC's. Detailed description, analysis, and evaluation of the algorithm can be found in [27].

It is important to emphasize that although an implementation generally involves certain approximation due to lack of better algorithms for computation, the significance of the exact descriptions of grown regions by uncertainty, which is the main contribution of this paper, is by no means lessened. Quite on the contrary, the exact representation is a necessary benchmark against which different approximate representations can be evaluated and compared. The implemented algorithm in [27] demonstrates one such feasible approximation.

8 Conclusions

We have presented a novel method to exactly grow an arbitrary polyhedron by its location uncertainty, given its position and orientation uncertainty bounds. Based on the method, three types of regions of a polyhedral object have been introduced: the grown regions, the grown shell regions, and the core regions. Since the representations are exact, they give the least upper bounds of the corresponding regions.

These regions can be useful in many robotic tasks where the effect of uncertainties needs to be dealt with. In particular, by analyzing the intersections between the grown shell regions of two objects, the set of all principal contacts that may be formed due to location uncertainties between the two objects (in their current locations) can be obtained, serving as the basis from which more precise contact information can be extracted by additional sensing means. We have briefly introduced such an application and its implementation in this paper, more details of which can be found in [27].

The grown regions and core regions of objects can be used to prevent and predict collisions caused by uncertainties. For example, in planning a collision-free path[28] for a robot in a *crowded* environment, it might be necessary to consider the grown regions of the objects by location uncertainties so that a path planned can be guaranteed to be safe, i.e., collision-free, in spite of uncertainties. The exact representations of the grown regions ensure that the remaining free space is the largest guaranteed one taking into account uncertainties. The core regions of objects, on the other hand, can be used to predict guaranteed collisions: if an object at certain location will intersect the core region of an obstacle, then the object will definitely collide with the obstacle at that location in spite of the location uncertainty of the obstacle.

Much more can be done as future extensions of the work reported in this paper. Growing an object element by element provides, in addition to its advantages that we have already shown, great flexibility for possible extensions and/or improvements of the current method. For instance, one may consider different uncertainty parameters (values) depending on surface elements. One may also consider the uncertainties as Gaussian distributions or some other probabilistic distributions rather than error bounds, under which the grown objects could be more useful. The method can also be generalized to growing special-shape non-polyhedra such as cylindrical, conical, or spherical objects, as well as objects with combined special shapes.

An important future task is to study good computer representations (approximations) of the exact grown regions described in this paper and efficient algorithms to build such representations and to reason about the intersections between two such regions. The algorithm described in [27] demonstrates one such attempt. Different approximations should then be compared against the exact representation in order to have their merits evaluated.

Acknowledgements

The authors would like to thank the anonymous reviewers and the editors for their insightful comments and their review effort.

References

- [1] A.P. Ambler and R.J. Popplestone. Inferring the positions of bodies from specified spatial relationships. *Artificial Intelligence*, 6(2):157–174, 1975.
- [2] H. Asada and S. Hirai. Towards a symbolic-level force feedback: Recognition of assembly sequence states. In *Proc. Int. Symp. Robotics Res.*, pages 290–295, 1989.
- [3] J. W. Boyse. Interference detection among solids and surfaces. *Communications of the ACM*, 22(1):3–9, 1979.

- [4] R. Desai. *On Fine Motion in Mechanical Assembly in Presence of Uncertainty*. PhD thesis, Department of Mechanical Engineering, the University of Michigan, 1989.
- [5] R. Desai and R. Volz. Identification and verification of termination conditions in fine motion in presence of sensor errors and geometric uncertainties. In *IEEE Int. Conf. on Robotics and Automation*, pages 800–807, 1989.
- [6] H.A. ElMaraghy and S. Payandeh. Contact prediction and reasoning for compliant robot motions. *IEEE Trans. Robotics and Automation*, 5(4):533–538, August 1989.
- [7] A.O. Farahat, P.F. Stiller, and J.C. Trinkle. On the algebraic geometry of contact formation cells for systems of polygons. In *Proc. IEEE International Conference on Robotics and Automation*, pages 3028–3029, San Diego, CA, May 1994.
- [8] E.G. Gilbert, D.W. Johnson, and S.S. Keerthi. A fast procedure for computing the distance between complex objects in three-dimensional space. *IEEE Journal of Robotics and Automation*, 4:193–203, April 1988.
- [9] A. Giraud and D. Sidobre. Contact manipulation and geometric reasoning. In J.-D. Boissonnat and J.-P. Laumond, editors, *Geometry and Robotics*. Springer-Verlag, 1989.
- [10] G.J. Hamlin, R.B. Kelley, and J. Tornerio. Efficient distance calculation using the spherically-extended polytope (s-tope) model. In *IEEE Int. Conf. Robotics and Automation*, pages 2502–2507, Nice, France, May 1992.
- [11] S. Hirai and K. Iwata. Recognition of contact state based on geometric model. In *IEEE Int. Conf. on Robotics and Automation*, pages 1507–1512, Nice, France, May 1992.
- [12] H. Hirukawa, T. Matsui, and K. Takase. Automatic determination of possible velocity and applicable force of frictionless objects in contact from a geometric model. *IEEE Transactions on Robotics and Automation*, 10(3):309–321, June 1994.
- [13] K. Ikeuchi and T. Suehiro. Toward an assembly plan from observation, part i: Task recognition with polyhedral objects. *IEEE Transactions on Robotics and Automation*, 10(3):368–385, June 1994.
- [14] C. Laugier. Planning fine motion strategies by reasoning in the contact space. In *IEEE Int. Conf. on Robotics and Automation*, pages 653–659, May 1989.
- [15] T. Lozano-Pérez. Spatial planning: A configuration space approach. *IEEE Trans. Comput.*, C-32(2):108–120, 1983.

- [16] T. Lozano-Pérez and M. A. Wesley. An algorithm for planning collision-free paths among polyhedral obstacles. *Commun. ACM*, 22(10):560–570, 1979.
- [17] N. Mimura and Y. Funahashi. Parameter identification of contact conditions by active force sensing. In *Proc. IEEE International Conference on Robotics and Automation*, pages 2645–2650, San Diego, CA, May 1994.
- [18] A. A. G. Requicha. Toward a theory of geometric tolerancing. *The International Journal of Robotics Research*, 2(4):45–60, 1983.
- [19] Jr. R.H. Sturges. A three dimensional assembly task quantification with application to machine dexterity. *Int. J. Robotics Res.*, 7(4):34–78, August 1988.
- [20] M. Spreng. Dealing with unexpected situations during the execution of robot motions. In *Proc. IEEE International Conference on Robotics and Automation*, pages 64–69, Sacramento, CA, May 1991.
- [21] F. Thomas and C. Torras. Interference detection between non-convex polyhedra revisited with a practical aim. In *IEEE ICRA*, pages 587–594, May 1994.
- [22] J. Tornero, G.J. Hamlin, and R.B. Kelley. Spherical-object representation and fast distance computation for robotic applications. In *IEEE Int. Conf. Robotics and Automation*, pages 1602–1607, Sacramento, CA, April 1991.
- [23] J. Xiao. Replanning with compliant rotations in the presence of uncertainties. In *IEEE Int. Symposium on Intelligent Control*, pages 102–107, August 1992.
- [24] J. Xiao. Automatic determination of topological contacts in the presence of sensing uncertainties. In *IEEE Int. Conf. Robotics and Automation*, pages 65–70, Atlanta, May 1993.
- [25] J. Xiao and M. Su. Automatic verification of principal contacts using vision. In *IEEE Int. Symposium on Intelligent Control*, pages 314–319, August 1993.
- [26] J. Xiao and R. Volz. On replanning for assembly tasks using robots in the presence of uncertainties. In *IEEE Int. Conf. Robotics and Automation*, pages 638–645, 1989.
- [27] J. Xiao and L. Zhang. A general algorithm to determine geometrically valid contact formations from possible contact primitives. In *IEEE Int. Conf. Robotics and Automation*, pages 2728–2733, Nagoya, Japan, May 1995.
- [28] C.-K. Yap. Algorithmic motion planning. In J.T. Schwartz and C.-K. Yap, editors, *Advances in Robotics, Vol. 1: Algorithmic and Geometric Aspects of Robotics*, pages 95–143. Lawrence Erlbaum Associates, 1987.

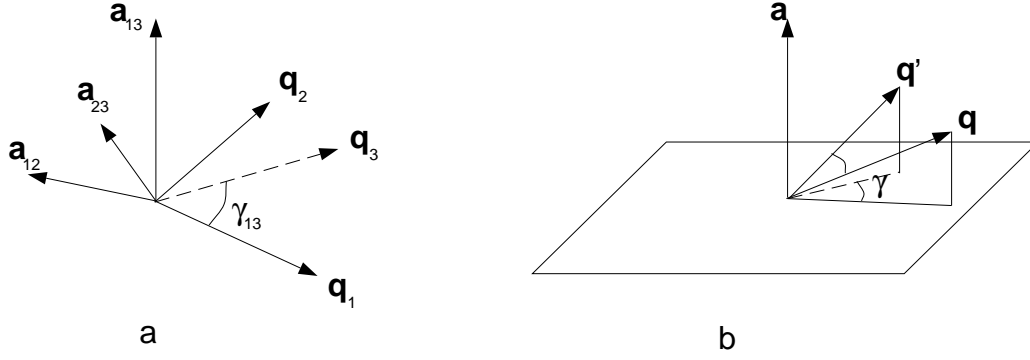


Figure 22: Vectors $\mathbf{q}_1, \mathbf{q}_2, \mathbf{q}_3$ and the rotation axes

A. Proof that D_o Is a Metric

Let M_1, M_2, M_3 denote 3×3 rotation matrices. D_o is defined as $D_o(M_1, M_2) = |\gamma|$, where γ satisfies $Rot(\mathbf{a}, \gamma) = M_1^T M_2$, $\gamma \in [-\pi, \pi]$, and \mathbf{a} denotes the axis of rotation. To show that D_o is a metric, we need to prove the following:

1. $D_o(M_1, M_2) \geq 0$ and iff $M_1 = M_2$, $D_o(M_1, M_2) = 0$.
2. $D_o(M_1, M_2) = D_o(M_2, M_1)$.
3. $D_o(M_1, M_2) + D_o(M_2, M_3) \geq D_o(M_1, M_3)$.

First, the definition of D_o gives $D_o(M_1, M_2) \geq 0$, and since

$$\gamma = 0 \iff M_1^T M_2 = Rot(\mathbf{a}, 0) = I_{3 \times 3} \iff M_1 = M_2$$

where $I_{3 \times 3}$ is the identity matrix, we know that iff $M_1 = M_2$, $D_o(M_1, M_2) = 0$.

Secondly, since

$$M_1^T M_2 = (M_1^T M_2)^{-1} = Rot^{-1}(\mathbf{a}, \gamma) = Rot(\mathbf{a}, -\gamma)$$

we have $D_o(M_2, M_1) = D_o(M_1, M_2) = |\gamma|$.

Finally, let $Rot(\mathbf{a}_{12}, \gamma_{12}) = M_1^T M_2$, $Rot(\mathbf{a}_{23}, \gamma_{23}) = M_2^T M_3$, $Rot(\mathbf{a}_{13}, \gamma_{13}) = M_1^T M_3$. Let \mathbf{q}_1 be a vector which is perpendicular to \mathbf{a}_{13} and fixed in the frame whose orientation is represented by M_1 . The rotations $Rot(\mathbf{a}_{12}, \gamma_{12})$ and $Rot(\mathbf{a}_{13}, \gamma_{13})$ rotate \mathbf{q}_1 to \mathbf{q}_2 and to \mathbf{q}_3 respectively. The rotation $Rot(\mathbf{a}_{23}, \gamma_{23})$ rotates \mathbf{q}_2 to \mathbf{q}_3 (Fig. 22a). We know the fact that iff when a vector \mathbf{q} is perpendicular to the rotation axis \mathbf{a} , the angle between \mathbf{q} and its new position after a rotation of angle γ can reach its maximum value γ (Fig. 22b). Thus, since \mathbf{q}_1 is perpendicular to \mathbf{a}_{13} , but \mathbf{q}_1 and \mathbf{q}_2 may not be perpendicular to \mathbf{a}_{12} and \mathbf{a}_{23} , we have

$$|\gamma_{13}| = \angle(\mathbf{q}_1, \mathbf{q}_3), \quad |\gamma_{12}| \geq \angle(\mathbf{q}_1, \mathbf{q}_2), \quad |\gamma_{23}| \geq \angle(\mathbf{q}_2, \mathbf{q}_3)$$

Also,

$$\angle(\mathbf{q}_1, \mathbf{q}_2) + \angle(\mathbf{q}_2, \mathbf{q}_3) \geq \angle(\mathbf{q}_1, \mathbf{q}_3)$$

Combining the above equations, we have

$$|\gamma_{12}| + |\gamma_{23}| \geq |\gamma_{13}|$$

that is, $D_o(M_1, M_2) + D_o(M_2, M_3) \geq D_o(M_1, M_3)$. \blacksquare

B. Derivation of Equation (5)

Equation (5) describes the boundary circle $l(q)$ of the grown region \mathcal{Q}_o of a point q on e , as shown in Fig. 10, in terms of the spherical coordinates (r, θ, ϕ) (Fig. 9).

Let (x, y, z) denote a point on $l(q)$ with spherical coordinates (r, θ, ϕ) . Thus,

$$\begin{cases} x = r \sin \theta \cos \phi \\ y = r \sin \theta \sin \phi \\ z = r \cos \theta \end{cases} \quad (13)$$

Let (x_q, y_q, z_q) be the Cartesian coordinates of the point q . Since the spherical coordinates of q are $(d_e / \sin \beta, \beta, 0)$ (see Fig. 10), by Theorem 3,

$$r = d_e / \sin \beta.$$

Consequently, the following holds:

$$\begin{cases} x_q = r \sin \beta \\ y_q = 0 \\ z_q = r \cos \beta. \end{cases} \quad (14)$$

From Theorem 3, the center (x_c, y_c, z_c) of the circle $l(q)$ is at $\cos \epsilon_o \mathbf{p}$, that is,

$$\begin{cases} x_c = r \cos \epsilon_o \sin \beta \\ y_c = 0 \\ z_c = r \cos \epsilon_o \cos \beta. \end{cases} \quad (15)$$

The radius of $l(q)$ is $r \sin \epsilon_o$. Thus $l(q)$ satisfies the equation:

$$\begin{cases} (x - x_c)^2 + (y - y_c)^2 + (z - z_c)^2 = r^2 \sin^2 \epsilon_o \\ r = d_e / \sin \beta \end{cases} \quad (16)$$

From equations (13) and (15), the first equation in (16) can be represented in spherical coordinates as:

$$(\sin \theta \cos \phi - \cos \epsilon_o \sin \beta)^2 + \sin^2 \theta \sin^2 \phi + (\cos \theta - \cos \epsilon_o \cos \beta)^2 = \sin^2 \epsilon_o.$$

which can be reduced to

$$\cos \phi = \frac{\cos \epsilon_o - \cos \theta \cos \beta}{\sin \theta \sin \beta}. \quad (17)$$

Note that for $\beta \leq \pi/2$,

$$\begin{cases} \sin \beta = \frac{d_e}{r} \\ \cos \beta = \frac{\sqrt{r^2 - d_e^2}}{r}. \end{cases} \quad (18)$$

From (18) and (17), the first equation in (5) can be easily derived.

C. Theorem 10 and Proof

Let P_1 and P_2 be two polyhedral objects in contact. If one of the objects, say, P_1 , is assumed to be fixed, then the following theorem holds.

Theorem 10. Suppose P_1 is fixed at a known location. Let ϵ_p and ϵ_o be the position and orientation uncertainties of P_2 respectively. Let $\mathcal{S}_{p,1}$ be the grown shell region of P_1 by ϵ_p and $\mathcal{S}_{o,2}$ be the grown shell region of P_2 by ϵ_o . Then, the intersection between $\mathcal{S}_{p,1}$ and $\mathcal{S}_{o,2}$ contains the information of all possible principal contacts between the original P_1 and P_2 , i.e., the information of \mathcal{S}_{pc} , taking into account the uncertainties.

Proof. We now show that for a fixed orientation of P_2 , represented by the rotation matrix 1M_2 with respect to the frame of P_1 , the position uncertainty ϵ_p of P_2 can be “transferred to” P_1 , so that growing P_1 by ϵ_p is equivalent to growing P_2 by ϵ_p . Let ${}^1\hat{\mathbf{p}}_2$ be the estimated or sensed value of ${}^1\mathbf{p}_2$, which is the position vector of P_2 with respect to the frame of P_1 . By Definition 1,

$$\|{}^1\hat{\mathbf{p}}_2 - {}^1\mathbf{p}_2\| \leq \epsilon_p.$$

Let ${}^2\mathbf{p}_1$ be the position vector of P_1 with respect to the actual frame of P_2 . Then,

$${}^2\mathbf{p}_1 = -({}^2M_1)^T({}^1\mathbf{p}_2),$$

where $({}^2M_1)^T$ is the transpose of 1M_2 . Let ${}^2\hat{\mathbf{p}}_1$ be:

$${}^2\hat{\mathbf{p}}_1 = -({}^2M_1)^T({}^1\hat{\mathbf{p}}_2).$$

Since $({}^2M_1)^T$ is a rotation matrix, $|({}^2M_1)^T| = 1$; thus

$$\|{}^2\hat{\mathbf{p}}_1 - {}^2\mathbf{p}_1\| = \|{}^1\hat{\mathbf{p}}_2 - {}^1\mathbf{p}_2\| \leq \epsilon_p,$$

which means that the fact that the position of P_2 with respect to P_1 has an uncertainty ϵ_p can be viewed equivalently as the position of P_1 with respect to P_2 has an uncertainty ϵ_p . In that sense, the position uncertainty of P_2 can be “transferred to” P_1 . Thus, for a fixed orientation of P_2 with respect to P_1 , all possible contacts between P_1 and P_2 due to ϵ_p can be obtained from the intersection between $\mathcal{S}_{p,1}$, the grown region of P_1 by ϵ_p , and P_2 at its estimated position ${}^1\hat{\mathbf{p}}_2$.

The orientation uncertainty of P_2 can be taken care of by growing P_2 by ϵ_o to obtain $\mathcal{S}_{o,2}$. The intersections between $\mathcal{S}_{p,1}$ and $\mathcal{S}_{o,2}$ contain the information of all possible contacts between P_1 and P_2 due to both uncertainties ϵ_p and ϵ_o . ■